THE JOURNAL OF PHYSICAL CHEMISTRY B

Article

pubs.acs.org/JPCB

Dynamics of Isolated Water Molecules in a Sea of Ions in a Room Temperature Ionic Liquid

Daryl B. Wong, Chiara H. Giammanco, Emily E. Fenn,† and Michael D. Fayer*

Department of Chemistry, Stanford University, Stanford, California 94305, United States

Supporting Information

ABSTRACT: The vibrational dynamics of the antisymmetric and symmetric stretching modes of very low concentration spatially isolated D_2O molecules in the room temperature ionic liquid (RTIL) 1-butyl-3-methylimidazolium hexafluorophosphate ($BmImPF_6$) were examined using two-dimensional infrared (2D IR) vibrational echo spectroscopy and infrared pump−probe experiments. In $BmImPF_6$, D_2O's antisymmetric and symmetric stretching modes are well resolved in the IR absorption spectrum in spite of the fact that the D_2O is surrounded by a sea of ions, making it is possible to study inter- and intramolecular dynamics. Both population exchange between the modes and excited-state relaxation to the ground state contribute to the population dynamics. The kinetics for the incoherent population exchange (scattering) between the two modes was determined by the time dependence of the exchange peaks in the 2D IR spectrum. In addition, coherent quantum beats were observed at short time in both the amplitudes and 2D IR band shapes of the modes. The quantum beat decay is caused by dephasing due to both inhomogeneous and homogeneous broadening of the spectral lines. Analysis of the oscillations of the 2D line shapes demonstrates that there is some degree of anticorrelation in the inhomogeneous broadening of the two modes. It is proposed that a distribution in the coupling strength between the local modes that give rise to symmetric and antisymmetric eigenstates is responsible for the anticorrelation. Spectral diffusion, caused by structural evolution of the medium, occurs on multiple time scales and is identical for the two modes within experimental error. The spectral diffusion is fast compared to the time scale for complete orientational randomization of the RTIL. Spectral diffusion of the OD stretch of HOD in $BmImPF_6$ was also measured, and is essentially the same as that of the D_2O modes. Orientational anisotropy measurements of HOD in $BmImPF_6$ determined the orientational relaxation dynamics of the isolated HOD molecules.

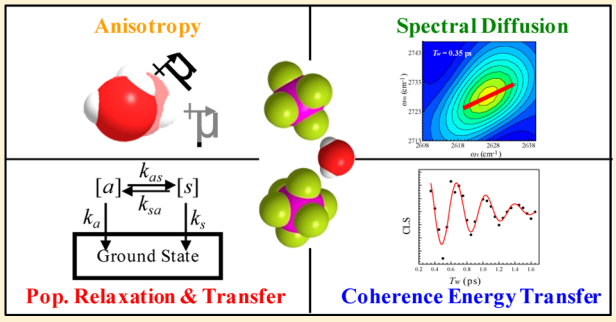

I. INTRODUCTION

Water plays an important role in mediating chemical, geological, and biological processes. In many if not most contexts, water is not in the form of a pure liquid, but interacts with other molecules, interfaces, and ions. The nature of water in salt solutions, such as NaBr or $MgSO_4$,[1−3] has been investigated extensively to understand the effects of the interactions of water with ions. However, salt solutions place a limit on the lowest concentration at which the properties of water interacting with ions can be studied. At sufficiently low water concentration, the salt will crystallize. In such studies, water interacts with ions but also with a large number of other water molecules.

Room temperature ionic liquids (RTIL), such as 1-butyl-3-methylimidazolium hexafluorophosphate ($BmImPF_6$), are salts that are liquids at room temperature. Because RTILs are themselves liquids, it is possible to study water interacting with ions at such low water concentrations that the water molecules are isolated in a sea of ions and not interacting with other water molecules. The ability to observe the dynamics of spatially isolated water molecules in an ionic liquid can contribute to a better understanding of water's fundamental intermolecular interactions with ions as well as the intramolecular dynamics of the isolated water molecules in condensed-phase systems.

The vibrational spectral region containing the hydroxyl stretches of water at low concentration in $BmImPF_6$ reveals two narrow spectrally resolved peaks far blue-shifted from their vibrational frequency in bulk water.[4−6] These peaks come from the symmetric and antisymmetric vibrational stretching modes of water. The splitting is ∼100 cm^{-1} and the line widths are ∼20 cm^{-1}. In the experiments presented here on D_2O, peak positions and the splitting, as well as the anharmonicities and combination band shift (found with 2D IR data), are relatively close to the gas-phase values.

The system of D_2O in $BmImPF_6$ permits a thorough examination of the internal dynamics of water's vibrational degrees of freedom and the external dynamics of isolated water with surrounding ions. 2D IR vibrational echo experiments and polarization selective pump−probe experiments are used to study D_2O as well as the OD stretch of HOD. Because the two

Received: October 11, 2012
Revised: December 27, 2012
Published: December 31, 2012

   dx.doi.org/10.1021/jp310086s | J. Phys. Chem. B 2013, 117, 623−635

modes of D_2O are well separated and resolved, both incoherent and coherent population transfer between them can be measured. Time constants for incoherent scattering between the modes, caused by absorption and emission of bath "phonons", were measured. The up and down rates obey detailed balance when the appropriate Bose factor is used. Coherent excitation transfer between the modes is observed in both pump−probe and 2D IR experiments. It is demonstrated that the decay of the observed short time oscillations is caused by a combination of the inhomogeneous and homogeneous broadening of the spectral lines that results in dephasing of the coherence transfer. The 2D IR bands also oscillate in shape. The shape oscillations are quantified using the center line slope (CLS) method,[7,8] and the analysis reveals that there is some degree of anticorrelation of the inhomogeneous broadening of the symmetric and antisymmetric lines. It is proposed that the anticorrelation is caused by a distribution in the strength of the coupling between the local modes that give rise to the symmetric and antisymmetric eigenstates.

2D IR vibrational echo experiments are used to measure the spectral diffusion of the two stretching modes of D_2O as well as the OD stretch of HOD in $BmImPF_6$. Spectral diffusion reports on the structural dynamics of the medium. Spectral diffusion is analyzed using the CLS method[7,8] to obtain the frequency−frequency correlation function (FFCF), which provides time scale and amplitude information on the dynamics. The FFCFs for all three modes have multiple components that are almost the same. The decay of the FFCF is much faster than the complete orientational randomization of the RTIL structure measured with optical heterodyne detected optical Kerr effect experiments.[9] Polarization-selective pump−probe experiments were used to measure the HOD orientational relaxation because excitation exchange between the modes of D_2O interferes with the orientational relaxation measurement. It was found that the orientational relaxation is faster than the decay of the FFCF.

Previous studies have examined the very short time dynamics of spatially isolated water molecules in acetonitrile.[10,11] These experiments examine intramolecular coherent excitation exchange between the two water vibrational modes, which give spectral beats in the data. Such coherent exchange is also studied for the RTIL/D_2O system. In the previous studies,[10,11] the symmetric and antisymmetric hydroxyl bands are relatively wide, leading to substantial overlap of the peaks in the absorption spectrum. The widths of the bands in the 2D IR spectra cause substantial overlap, which complicates the data analysis although considerable insight into the acetonitrile/water system was obtained. Here, because the symmetric and antisymmetric hydroxyl stretch absorptions are narrow, the bands in the 2D IR spectrum do not overlap, which helps in the detailed analysis of coherent excitation exchange between the modes.

II. EXPERIMENTAL DETAILS

A. Sample Preparation. 1-Butyl-3-methylimidazolium hexafluorophosphate (Iolitec Ionic Liquids Technologies GmbH) was heated and vacuum pumped to remove excess water from the ionic liquid. D_2O (Acros Organics) was added to BmIm PF_6 in a close to H_2O-free atmosphere to create solutions of 24 BmImPF6:1 D_2O. Water content was confirmed by Karl Fischer titration. Samples were transferred to a sample cell and held between two calcium fluoride plates separated by a 250 μm thick spacer to achieve an absorbance of ∼0.2−0.3.

B. Spectroscopy and Data Analysis. Linear FT-IR absorption spectra were acquired at 2 cm^{-1} resolution. A detailed description of the laser system and the experimental details regarding the polarization sensitive pump−probe and 2D IR vibrational techniques are reported in previously published work.[12] The laser system was tuned to create ∼70 fs mid-infrared pulses centered at 2680 cm^{-1} with a full width at half-maximum (fwhm) of 200 cm^{-1}.

In the 2D IR vibrational echo experiment, three time-ordered IR pulses impinge on the sample, and the sample response gives rise to a fourth pulse, the vibrational echo that emerges from the sample in a wave vector matched direction. The vibrational echo pulse is overlapped with another pulse, the local oscillator (LO). The temporal interference between the vibrational echo pulse and the local oscillator provides phase information necessary to perform Fourier transforms to obtain the 2D spectra. The time delay between pulses 1 and 2 is called τ, and the delay between pulses 2 and 3 is called T_w. The echo pulse is emitted a time t after the third pulse. The combined echo and LO pulses are passed through a monochromator acting as a spectrograph and detected with a 32-element array MCT array detector. The spectrograph does one of the two Fourier transforms and provides the vertical axis (ω_m axis) of the 2D spectrum. When τ is scanned, a temporal interferogram is produced at each detected wavelength. Numerical Fourier transformation of these interferograms gives the horizontal axis (ω_τ axis) of the 2D spectrum.

In a 2D IR vibration echo experiment, τ is scanned for fixed T_w, and a 2D spectrum is obtained. Then T_w is changed, and τ is scanned to obtain another 2D spectrum. A series of such spectra are recorded. The desired information is contained in the peak positions and the T_w dependence of the amplitudes and shapes of the peaks in the 2D spectrum.

In the pump−probe experiment, two pulses, a strong pump and a weak probe, impinge on the sample. The time between the two pulses is t. The pump produces a transient change in the transmission of the probe. The probe is frequency resolved by the spectrograph/array detector, and its amplitude at each frequency is measured as a function of t. The change in probe transmission is obtained with the probe polarization parallel and perpendicular to the pump.

1. Polarization Selective Pump−Probe Analysis. The polarization selective pump−probe technique tracks the decay of the probe with polarizations parallel ($I_\parallel$) and perpendicular ($I_\perp$) to the pump pulse. The data contain information about both population and orientational dynamics.

$$I_\parallel = P(t)(1 + 0.8C_2(t)) \tag{1}$$

$$I_\perp = P(t)(1 - 0.4C_2(t)) \tag{2}$$

$P(t)$ is the vibrational population and $C_2(t)$ is the second Legendre polynomial which is the orientational correlation function for the vibrational mode. Population relaxation can be obtained by combining the parallel and perpendicular signals

$$3P(t) = I_\parallel + 2I_\perp \tag{3}$$

Both parallel and perpendicular signals are also used to extract the orientational anisotropy, $r(t)$, which is related to the orientational correlation function by

$$r(t) = \frac{I_\parallel - I_\perp}{I_\parallel + 2I_\perp} = 0.4C_2(t) \tag{4}$$

dx.doi.org/10.1021/jp310086s | J. Phys. Chem. B 2013, 117, 623−635

2. 2D IR Vibrational Echo Signal Analysis. The 2D lineshape evolution was monitored as a function of T_w on two time scales: short time observation of coherent excitation transfer oscillating between the two coupled modes and a longer time scale indicative of structural evolution of the environments surrounding the D_2O molecules. The FFCF, which quantifies the spectral diffusion in terms of amplitudes and time scales of dynamics, is the joint probability that a vibration with an initial ($t = 0$) frequency in the inhomogeneous spectral distribution will maintain its frequency at a later time t, averaged over all initial frequencies. To extract the FFCF from the 2D spectra, center line slope (CLS) analysis was employed.[7,8] The decay of the CLS was monitored at short time to track the frequency oscillations induced by coherence transfer and at longer times to determine the rates of spectral diffusion.

The FFCF is described with a multiexponential model

$$C_1(t) = \langle \delta\omega_{1,0}(\tau_1)\delta\omega_{1,0}(0)\rangle = \sum_i \Delta_i^2 \exp(-t/\tau_i) \tag{5}$$

where the Δ_i are the frequency fluctuation amplitudes of each component and the τ_i are their associated time constants. For a component of the FFCF where $\Delta\tau < 1$, the component is motionally narrowed, and it is the dominant source of the homogeneous broadening of the absorption line. When a component is motionally narrowed, Δ and τ cannot be determined separately. The motionally narrowed homogeneous contribution to the absorption spectrum has a pure dephasing width given by $\Gamma^* = \Delta^2\tau = 1/\pi T_2^*$, where T_2^* is the pure dephasing time and Γ^* is the pure dephasing line width. The observed homogeneous dephasing time, T_2, also has contributions from the vibrational lifetime and orientational relaxation:

$$\frac{1}{T_2} = \frac{1}{T_2^*} + \frac{1}{2T_1} + \frac{1}{3T_{or}} \tag{6}$$

where T_1^*, T_1, and T_{or} are the pure dephasing time, vibrational lifetime, and orientational relaxation times, respectively. The total homogeneous line width is then $\Gamma = 1/\pi T_2$.

III. LINEAR ABSORPTION AND 2D IR SPECTRA OF D_2O IN BMIMPF$_6$

Figure 1 displays the linear IR absorption spectrum of the two vibrational modes of isolated D_2O molecules in BmImPF$_6$. Gaussian fits to the two major peaks in the absorption spectrum show that the symmetric stretch is centered at 2627 cm^{-1} with a fwhm of 17 cm^{-1} and the antisymmetric stretch is centered at 2726 cm^{-1} with a fwhm of 24 cm^{-1}. The peak positions are close to the gas phase values of D_2O (ν_a = 2788 cm^{-1}, ν_s = 2671 cm^{-1}).[13] Because the sample is not completely free of H_2O, the spectrum also shows a small peak that is the OD stretch of HOD centered at 2678 cm^{-1}, which is about half way between the antisymmetric and symmetric stretching peaks. As the water molecules in the RTIL solution are spatially isolated, the presence of HOD does not have an effect on the D_2O molecules.

In some of the experiments the OD stretch of HOD was studied. For these experiments, the overall water concentration (D_2O + H_2O) relative to BmImPF$_6$ was held constant, but the fraction of H_2O was increased to increase the size of the OD peak. Figure S1A in the Supporting Information shows the FT-IR spectrum of the OD stretching peak between the D_2O antisymmetric and symmetric peaks. The OD peak has a fwhm of 21 cm^{-1}. For comparison, the OD stretch of HOD in bulk H_2O is 170 cm^{-1} fwhm and it is shifted by ~180 cm^{-1} to lower frequency (see Figure S1B). The shift to lower frequency of the OD stretch of HOD in H_2O compared to its frequency in BmImPF$_6$ shows that hydroxyls interact with this ionic environment much more weakly than they do with other water molecules. Such blue shifts of the hydroxyl stretch when interacting with anions has been interpreted as arising from weak hydrogen bond strengths and weak local electric fields produced by the anions along the hydroxyl.[14] In addition, the narrow width of the OD band in the RTIL shows that the range of environmental influences on the frequency experienced by the hydroxyl when interacting with ions is much less than when the hydroxyl is interacting with other water molecules.

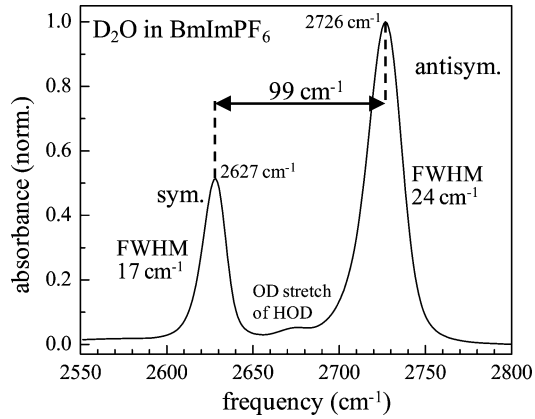

Figure 1. Background-subtracted FT-IR spectrum of D_2O in BmImPF$_6$. The antisymmetric stretching mode peak is centered at 2726 cm^{-1} (fwhm of 24 cm^{-1}). The symmetric stretch is centered at 2627 cm^{-1} (fwhm of 17 cm^{-1}).

Previous linear infrared absorption studies of trace water in BmIm ionic liquids displayed a strong dependence of the hydroxyl stretching frequency on the anion.[5] The frequency shift of the hydroxyl stretching modes in H_2O with BmImPF$_6$ were found to be less than 90 cm^{-1} red-shifted from the gas-phase values with a hydrogen bond enthalpy of −1.8 kcal/mol. Infrared studies and electronic structure calculations have shown that water molecules at low concentration in BmIm ionic liquids preferentially interact with the anions. The form of these interactions is A···HOH···A.[5,15,16] Such a molecular picture is consistent with the observation of two well-resolved peaks in the IR spectrum, corresponding to the two stretching modes of D_2O. The observation of a single OD peak for HOD (see Figure S1A) that is centered approximately between the two peaks of D_2O supports the proposition that the two peaks shown in Figure 1 are the antisymmetric and symmetric vibrational stretching eigenmodes. The relatively narrow line width of the OD of HOD in the RTIL shows that the local mode frequencies are quite similar.

The frequency splitting between the two D_2O modes is significant and similar to that observed in the gas phase. The energies of the antisymmetric (a) and symmetric (s) modes are

$$E_{a,s} = \frac{\hbar\omega_1 + \hbar\omega_2 \pm \sqrt{4J^2 + (\hbar\omega_1 - \hbar\omega_2)^2}}{2} \tag{7a}$$

where $\hbar\omega_1$ and $\hbar\omega_2$ are the energies of the local hydroxyl stretching modes and J is the coupling between the two local modes. In the strong coupling regime, the energies for the antisymmetric and symmetric stretch reduce to

dx.doi.org/10.1021/jp310086s | J. Phys. Chem. B 2013, 117, 623−635

$$E_{a,s} = \frac{\hbar\omega_1 + \hbar\omega_2}{2} \pm J \tag{7b}$$

Strong coupling occurs when $4J^2 \gg (\hbar\omega_1 - \hbar\omega_2)^2$ in eq 7a. From the peak splitting (see Figure 1), $J \sim -50$ cm^{-1}, and $4J^2 =$ ~10 000 cm^{-1}. The line width of the OD local mode (Supporting Information, Figure S1A) gives an approximate range for possible differences in the energies of the OD local modes for D_2O. The 2D IR vibrational echo experiments show there is a substantial homogeneous component to all of the absorption bands. The inhomogeneous contributions (fwhm) are ~16 cm^{-1}. The differences in the local mode energies can range from zero to ~20 cm^{-1} with a nonnegligible probability. However, because the coupling term $4J^2$ is large, $(\hbar\omega_1 - \hbar\omega_2)^2$ will be negligible by comparison, and the system can be taken to be in the strong coupling regime.

The anion has a significant effect on the hydroxyl stretching modes' frequencies, but the cation does not.[5,6] Longer cation alkyl chain lengths do not cause frequency changes in the water stretching modes,[17] which has been interpreted as evidence that the water molecules are located in ionic regions[5,6] and that the water molecule hydroxyl groups hydrogen bond only with anions.

While a one-dimensional spectrum displays vibrational modes in the system, a more detailed investigation of the coupling and interactions between the modes can be made using a nonlinear two-dimensional experiment.[18−22] The 2D IR vibrational echo experiments and IR pump−probe experiments conducted in this study access vibrational stretching eigenmodes of D_2O and their overtones. As a result, there are six peaks corresponding to one and two quanta transitions of vibrational energy levels in the system (see Figure 2). A detailed discussion of the unitary transformation of the Hamiltonian for a system of coupled local modes to a more delocalized basis has been covered extensively elsewhere[23−25] as has the effect of the interactions of the bath on vibrationally coupled systems.[26,27] It should be emphasized that the energy levels do not reflect the energy levels of the system in a normal mode or local mode basis. Instead, the system is described with respect to its observed eigenstates, which accounts for the effects of the bath coupled to the system (as in ref 27). The terms antisymmetric and symmetric stretches are used in describing these bath renormalized modes. It is also possible to describe a system such as D_2O studied here beginning in a local mode basis set as has been done previously for isolated H_2O molecules in acetonitrile.[10,11]

Information regarding the transitions between energy levels as well as the anharmonicities can be obtained directly from the analysis of a two-dimensional spectrum (Figure 2A).[22,27] Figure 2A shows a 2D IR spectrum of the system taken at T_w = 10 ps containing a total of 14 peaks. Two of the peaks located on the vertical line with ω_τ = 2678 cm^{-1} correspond to the 0 → 1 and 1 → 2 transitions of the OD stretch of small amounts of HOD in the solution. The other 12 peaks arise from the transitions of the symmetric and antisymmetric stretching modes of D_2O in $BmImPF_6$.

Figure 2B displays the transitions between energy levels of symmetric and antisymmetric eigenstates of D_2O in $BmImPF_6$. The value, i.e. (1*a*), in parentheses labels the transition in Figure 2B and the corresponding peak in the 2D IR spectrum in Figure 2A. $\nu_{0,0\to0,a}$ = 2726 cm^{-1} (1*a*); $\nu_{0,a\to0,2a}$ = 2681 cm^{-1} (2*a*); $\nu_{0,a\to s,a}$ = 2550 cm^{-1} (3*a*); $\nu_{s,0\to s,0}$ = 2627 cm^{-1} (1*s*); $\nu_{s,0\to2s,0}$ = 2573 cm^{-1} (2*s*); and $\nu_{s,0\to s,a}$ = 2649 cm^{-1} (3*s*). The

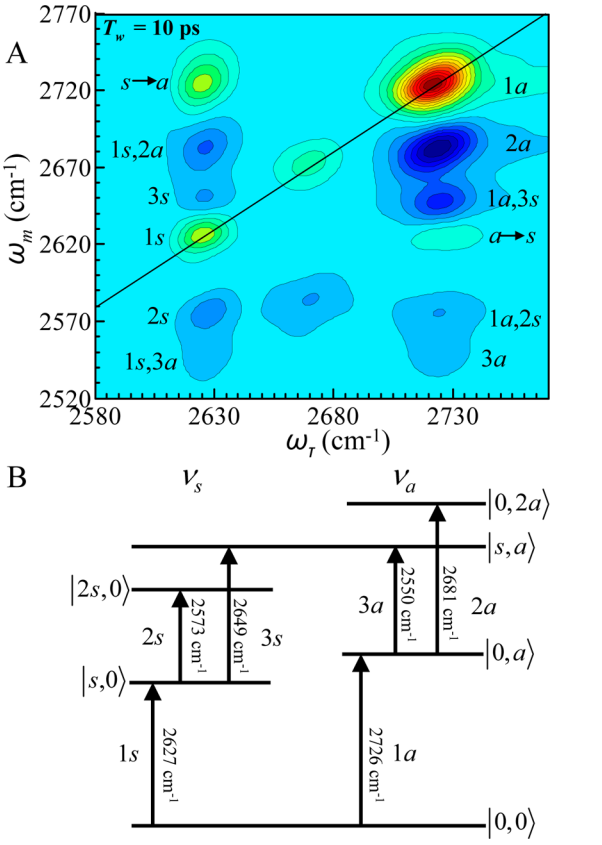

Figure 2. (A) 2D IR spectrum of D_2O in $BmImPF_6$. The peaks are labeled according to transitions in part B and described in the text. Peaks indicating coherence transfer between 1*a* and 1*s* vibrational modes are labeled s → a and a → s. Peaks which arise from population transfer between vibrational modes are indicated by labels with two transitions, i.e., 1*a*,3*s*, where 1*a* would be the first populated transition and 3*s* indicates echo emission from that labeled vibrational transition. The two unlabeled peaks in the middle of the plot arise from the 0 → 1 and 1 → 2 transitions of the OD stretch of residual HOD in solution. (B) Vibrational energy levels of D_2O in $BmImPF_6$ where ν_s and ν_a correspond to the symmetric and antisymmetric vibrational modes of D_2O, respectively. Each transition is indicated by a transition frequency (cm^{-1}) and an alphanumeric label, where *a* indicates the antisymmetric manifold and *s* indicates the symmetric manifold.

anharmonicity, the deviation of the vibrational potential from harmonic, of the symmetric stretch is X_{ss} = 54 cm^{-1}, while that of the antisymmetric stretch is X_{aa} = 45 cm^{-1}. The combination band shift, X_{as} = 77 cm^{-1}. All of the static spectroscopic parameters are given in Table 1.

The transitions shown by the arrows in Figure 2B give rise to half of the D_2O peaks displayed in Figure 2A. The other six off-diagonal peaks reflect intermode transitions between antisymmetric and symmetric vibrational manifolds. These peaks arise from interactions of radiation fields with both vibrational manifolds or when the two types of modes are coupled either

Table 1. Spectroscopic Parameters from FT-IR and 2D IR Measurements

mode	center (cm^{-1})	fwhm (cm^{-1})	anharm (cm^{-1})	comb shift
antisym	2726	24	45	77
sym	2627	17	54	77
OD of HOD	2678	21	90	N/A

dx.doi.org/10.1021/jp310086s | J. Phys. Chem. B 2013, 117, 623−635

through anharmonic terms in the intramolecular potential or through coupling to the bath (solvent) degrees of freedoms. The intramolecular coupling gives rise to coherent vibrational excitation exchange between the modes, while the coupling to the bath generates incoherent excitation exchange. More details of the interactions necessary to produce all 12 D_2O peaks in the 2D spectrum[28] are provided in Figures S2 and S3 in the Supporting Information, which show the rephasing double-sided Feynman diagrams that describe each quantum pathway.

The peaks labeled $s \rightarrow a$ and $a \rightarrow s$ in Figure 2A have contributions from three quantum pathways. (1) Excitation of one mode by the first pulse, stimulated emission to the ground state by the second pulse, and excitation of the other mode by the third pulse (Figure S2B, diagram i). (2) Excitation of both modes by the first two pulses followed by stimulated emission by the third pulse (Figure S2B, diagram j). These are two contributions, one of which gives only population to the peaks (Figure S2B, diagram i) while the other (Figure S2B, diagram j) involves coherent exchange of excitation between the two modes which produces quantum beating oscillations at the frequency of the difference between energy levels. The oscillations will be discussed in detail in section VI. (3) Incoherent population transfer between the two modes that is induced by absorption and emission of bath phonons (Figure S3C).[29] The first two pulses produce population of one mode followed by incoherent transfer of population to the other mode during T_w, and echo emission from the first excited state of the other mode stimulated by the third pulse. The off-diagonal peaks labeled 1*s*,2*a* and 1*a*,2*s* in Figure 2A, and those labeled 1*s*,3*a* and 1*a*,3*s*, also come from incoherent population transfer during T_w (Figure S3, 1x → 2y and 1x → xy, respectively). However, upon transfer to the other vibrational mode, the third pulse puts the system into a second excited state (1*s*,2*a* and 1*a*,2*s*) or a combination band (1*s*,3*a* and 1*a*,3*s*). Emission comes from these two excited states. The kinetics of the incoherent scattering process is discussed in section IV.

It should be noted that the system can be analyzed in a local mode basis and depending on the information desired[27] such an analysis can prove useful. However, because the observed energy eigenvalues of D_2O depend on bath interactions as well as the strength of coupling between local modes, the dynamics of the D_2O in $BmImPF_6$ are discussed in terms of the bath-renormalized eigenstates.

IV. POPULATION EXCHANGE AND VIBRATIONAL RELAXATION

Plots of the normalized vibrational population relaxation, $P(t)$, of the antisymmetric and symmetric peaks measured with IR pump−probe experiments are shown in Figure 3 (black curves, see eq 3). The antisymmetric mode population decays monotonically, but the symmetric stretch population shows an initial growth. The observed decay kinetics are described by expressions containing terms for the population exchange between the two D_2O stretching modes as well as vibrational relaxation to the ground state (see Figure 3 inset). The antisymmetric (2725 cm^{-1}) and symmetric peaks (2626 cm^{-1}) were fit (blue and red curves in Figure 3) to biexponential decays of the form

$$P(t) = A_1 e^{-t/\tau_1} + A_2 e^{-t/\tau_2} \tag{8}$$

where A_i is the amplitude of the decay and τ_i is the associated time constant. The antisymmetric stretch decays with a fast

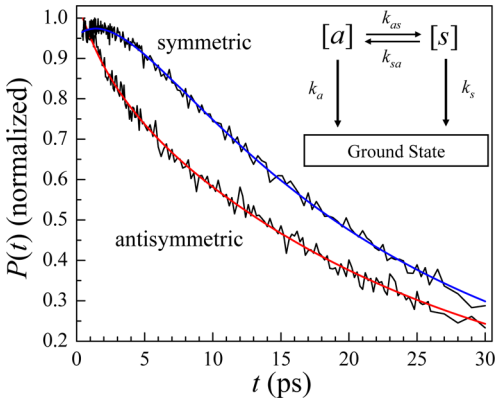

Figure 3. Population relaxation data for both the antisymmetric (2725 cm^{-1}) and symmetric (2626 cm^{-1}) peaks. Inset: the kinetic pathways for the excited antisymmetric and symmetric vibrational populations.

component of 2.1 ± 0.2 ps and a longer time constant of 22.5 ± 0.2 ps. The symmetric peak grows to a maximum with the same fast time constant, and then decays with the same long time constant. The excitation pulse is sufficiently broad to have essentially equal intensity at the absorption wavelengths of the two modes. However, the antisymmetric stretch has a larger amplitude (see Figure 1), and therefore, it has a larger initial population. The relaxation dynamics (Figure 3) are consistent with initial excited populations that are not in thermal equilibrium. Because the antisymmetric stretch has excess initial population, it will have an initial fast decay component, while the symmetric stretch will have an initial fast growth component. Fast exchange kinetics drive the excited-state populations to equilibrium, and then both populations decay slowly to the ground state. Because the vibrational lifetimes of both modes are slow compared to the rates of population exchange, the observed long time decay rate constants will be identical (22.5 ps) and the average of the individual rate constants that would occur in the absence of exchange. This value is in sharp contrast to the vibrational lifetime of the OD stretch of HOD in H_2O which is 1.8 ps.[30]

The fast decay constant obtained from the fit using eq 8 are only apparent time constants for the exchange processes. The results obtained from solving the following system of differential equations, which account for both exchange of populations and vibrational relaxation from each state, can be used to fit the pump−probe.

$$\frac{d[s]}{dt} = -(k_s + k_{sa})[s] + (k_{as})[a] \tag{9a}$$

$$\frac{d[a]}{dt} = -(k_a + k_{as})[a] + (k_{sa})[s] \tag{9b}$$

$[s]$ and $[a]$ are the populations of the symmetric and antisymmetric stretch, k_s and k_a are the vibrational lifetime decay rate constants of the symmetric and antisymmetric stretch, and k_{as} and k_{sa} are the exchange rate constants from $a \rightarrow s$ and $s \rightarrow a$, respectively. In fitting the pump−probe data to the kinetic model, the initial population values were set to $[a(0)] = 0.66$ and $[s(0)] = 0.33$ (the fit areas of each peak in the FT-IR spectrum). Solving this system of equations gives expressions for the observed amplitudes and time constants that involve the exchange and vibrational lifetime rate constants.

dx.doi.org/10.1021/jp310086s | J. Phys. Chem. B 2013, 117, 623−635

While it is possible to extract the actual scattering rates between the two modes by fitting the pump–probe data in Figure 3, the scattering up and down can be separated and observed independently using 2D IR data. The time dependent growth of the off-diagonal peaks labeled (1*a*,2*s*), (1*s*,2*a*), (1*a*,3*s*), and (1*s*,3*a*) in Figure 2A reflect the kinetics of the vibrational excitation population transfer that occurs between the two modes. Figure 4 plots data from two of the population

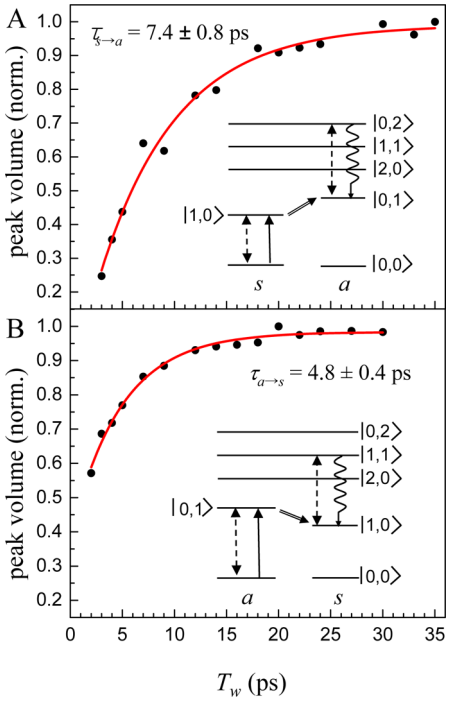

Figure 4. Incoherent population exchange data (black circles) for (A) the symmetric to the antisymmetric mode and (B) the antisymmetric to the symmetric mode. The red curves are fits to the data. Insets are energy diagrams showing the quantum pathways of each process, with *a* for antisymmetric and *s* for symmetric.

transfer peaks ((1*a*,3*s*) and (1*s*,2*a*)). The volume of each peak is plotted as a function of T_w. The data points are normalized to the maximum growth value. At sufficiently long time, these peaks will decay to zero amplitude. Inset in each data plot is a diagram illustrating the quantum pathways that give rise to the off-diagonal peaks employed in the analysis. The double arrow represents the incoherent scattering between the modes in Figure 4. These arrows are represented by the dashed lines in the two Feynman diagrams in Figure S3, A and B.

The antisymmetric to symmetric transfer peak grows in with a time constant of $\tau_{a\to s}$ = 4.8 ± 0.5 ps while the symmetric to antisymmetric scattering grows in with a time constant of $\tau_{s\to a}$ = 7.4 ± 0.8 ps. In determining these values, the vibrational lifetimes and the orientational relaxation rates were not included. However, the final population decay, 22.5 ps, is relatively long compared to the scattering times obtained from the fits. In addition, the orientational relaxation time, discussed below, is somewhat slower than the lifetime. The inclusions of the lifetimes and orientational relaxation influence the time dependence of the data in opposite directions. The vibrational lifetime causes the peaks to decay, which would effectively slow the buildup of the off-diagonal peaks. Usually, orientational relaxation also causes the peaks to decay. However, the symmetric and antisymmetric stretching modes' transition dipoles are perpendicular to each other, which causes orientational relaxation to increase the population exchange signal of the off-diagonal peaks. Given that the lifetime and the orientational relaxation are relatively slow and offset each other, these two processes will produce only a small error in the up and down scattering numbers reported above. In addition, using these values, the solutions to eqs 9a and 9b reproduced the pump–probe data without adjusting the time constants within experimental uncertainty. In these calculations, it is not possible to determine the individual vibrational lifetimes as the scattering is fast compared to both of them, which results in the same long time decays.

In the scattering process, energy must be conserved. Therefore, for $a \to s$, 100 cm^{-1} must be transferred to other modes of the system, and for $s \to a$, 100 cm^{-1} of energy must be taken up from other modes. Since D_2O does not have an internal 100 cm^{-1} mode, the energy comes from the bath. The RTIL solvent bath has 100 cm^{-1} modes[31,32] that are thermally populated at room temperature (k_BT = 206 cm^{-1}). The lowest order process involves cubic anharmonic coupling.[29] The coupling matrix element has a total of three creation and annihilation operators.[29] For $a \to s$ energy transfer, *a* is annihilated, *s* is created, and a 100 cm^{-1} bath mode is created. For $s \to a$, *s* is annihilated, *a* is created, and a 100 cm^{-1} bath mode is annihilated.

Because the coupling between initial and final molecular states as well as the density of bath states are the same for both the up and down scattering processes, the ratio of the down to up rate depends only on the phonon occupation number $K_{a\to s}/K_{s\to a} = (1 + n_p)/n_p$.[29] At room temperature, the Bose occupation number for a 100 cm^{-1} phonon, n_p = 1.6. Thus, for detailed balance to be obeyed, the ratio of the rate constants should be 1.63. The experimental ratio is 1.54, but given the error bars on the individual time constants, the ratio ranges from 1.75 to 1.33. Therefore, within experimental error, the up and down scattering rate constants obey detailed balance.

V. SPECTRAL DIFFUSION AND ORIENTATIONAL RELAXATION

The 2D IR experiments provide information on the structural dynamics of the $BmImPF_6$ solvent through the measurement of spectral diffusion. Spectral diffusion is manifested through changes in the diagonal band shapes with T_w. Changes in band shape are quantified using the CLS method,[7,8] which is then used to determine the FFCF.[28] The FFCF provides the homogeneous and inhomogeneous spectral components that make up the peaks in the IR absorption spectrum (Figure 1). Different solvent structures will result in different frequencies for the stretching modes. As the solvent structure evolves in time, the frequencies will change (spectral diffusion). At sufficiently long time, all structures will be sampled, and therefore, a molecule will sample all frequencies that give rise to the inhomogeneously broadened absorption spectrum. The FFCF yields the time scales and amplitudes of the frequency fluctuations experienced by the vibrational mode of interest.

Figure 5 displays the CLS data for the antisymmetric and symmetric stretching modes of D_2O as well as for the OD stretch of HOD. The CLS is the normalized FFCF. The offset from 1 at T_w = 0 is related to the homogeneous component of the absorption line. Combining the CLS data and the absorption spectrum yields the full FFCF including the homogeneous component (see discussion surrounding eqs 5 and 6).[7]

dx.doi.org/10.1021/jp310086s | J. Phys. Chem. B 2013, 117, 623–635

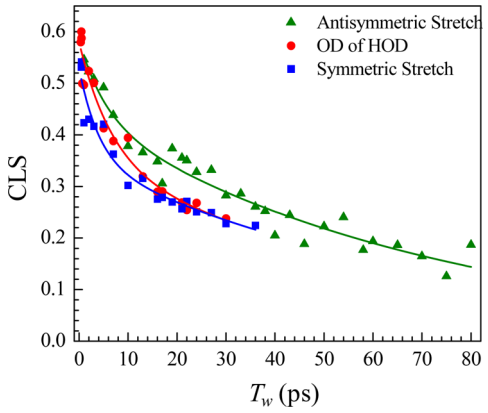

Figure 5. Spectral diffusion CLS decays (data points) from the antisymmetric and symmetric modes of D_2O and the OD stretch of 25% HOD/H_2O in $BmImPF_6$. The solid curves are fits with parameters given in Table 2.

Table 2 gives the FFCF parameters obtained using the multiexponential model for the FFCF (eq 5). Each of the FFCFs contains three components, a homogeneous component, and two inhomogeneous components. The slowest component, τ_2, is ~70 ps, and within the error bars, τ_2 is the same for all three modes. The associated Δ_2 is the amplitude of this component. The faster component of the spectral diffusion, τ_1, varies somewhat with the particular peak studied. However, within experimental error all three lines have the value of ~5 ps. Δ_1 is the associated amplitude. Γ is the homogeneous line width, with $\Gamma = 1/\pi T_2$. Γ and T_2 in Table 2 include contributions from pure dephasing, the vibrational lifetime, and orientational relaxation (see eq 6). However, because the lifetime and orientational relaxation (see below) are very slow, their combined contribution to Γ is ~0.4 cm^{-1}. The homogeneous line width is dominated by pure dephasing. Pure dephasing is caused by ultrafast structural fluctuations that sample the corresponding frequency range so fast motional narrowing occurs. Such ultrafast motions can only arise from the motions of very small structural components, such as small fluctuations in the distance between the PF_6^- anion and the hydrogen-bonded hydroxyl. Again, the homogeneous line widths of the three modes are very similar. The total absorption line width is the convolution of the total inhomogeneous Gaussian component with the Lorentzian component, Γ (fwhm). In Table 2, the inhomogeneous widths, Δ_i, are the standard deviations. The total inhomogeneous width is $(\Delta_1^2 + \Delta_2^2)^{1/2}$. The inhomogeneous fwhm is 2.35 times this number. Because Γ is comparable to the Gaussian component for each line, the overall line shape is a Voigt. While the data in Table 2 reproduces the CLS and the absorption spectra, the measurements are limited by the vibrational lifetimes and further limited by the very low concentration of D_2O and HOD in solution. Given the data shown in Figure 5 and the fits, a slower component a CLS amplitude of <0.05 cannot be ruled out.

It is important to note that, while incoherent population scattering between modes occurs, it does not affect the diagonal peak FFCFs because the scattering creates off-diagonal peaks, which do not contribute to the diagonal peak FFCF. Coherent excitation transfer can affect the diagonal peaks. However, it produces oscillations about an average value and the oscillation decay with ~1 ps time constant (see section VI).

In bulk water, the FFCF of the OD stretch of HOD in H_2O also has two spectral diffusion components of ~0.4 and 1.7 ps.[33,34] The fast component is caused by very local hydrogen bond fluctuations mainly in the length of the hydrogen bond, and the slower component is caused by complete structural randomization of the hydrogen bond network environment.[33,34] It is possible that the two spectral diffusion components in the FFCFs of the isolated D_2O and HOD in $BmImPF_6$ have an analogous origin. The faster ~5 ps component might arise from changes in the local structure of two anions bridged by the water and motions of the associated cations. As PF_6^- is much heavier than the water molecules surrounding an HOD in bulk water, the time scale for local structural fluctuations involving distance and angle can be substantially slower in the water/$BmImPF_6$ system than in bulk water. If the fast component of the FFCF reflects local structural changes, then in analogy to bulk water, distant larger structural rearrangement of the ions near a D_2O or HOD may give rise to the slower time scale component of the FFCF.

The slowest component of the FFCF can be compared to the time required for total orientational relaxation of the RTIL. Optical heterodyne detected optical Kerr effect (OHD-OKE) experiments have been used to study the orientational dynamics of RTILs from 100 fs to the time required for complete orientational randomization.[9,35] OHD-OKE experiments were conducted on $BmImPF_6$ at the low water content used in the IR experiments. The size of the OHD-OKE signal is determined by the polarizability and the polarizability anisotropy. Water produces negligible signal in these OHD-OKE measurements because of its very low concentration and small polarizability anisotropy. Because of its symmetry, isolated PF_6^- has no polarizability anisotropy. However, it can produce very short-lived and weak signals because of what are called interaction or collision-induced transient anisotropy. Therefore, the vast majority of the signal comes from the $BmIm^+$ cation with contribution from its alkyl chain.[9] Complete orientational relaxation of $BmIm^+$ requires complete structural randomization of the entire liquid.[9] The OHD-OKE measurements give a 2.3 ns time constant for the liquids structural randomization.

Given that the slowest component of the FFCF is ~70 ps, the dynamics that give rise to this time scale cannot be the due to the complete structural randomization of the liquid. In a

Table 2. FFCF Parameters for the Symmetric and Antisymmetric Stretching Modes of D_2O and the OD Stretch of Dilute HOD in $BmImPF_6$[a]

peak	T_2 (ps)	Γ (cm^{-1})	Δ_1 (cm^{-1})	τ_1 (ps)	Δ_2 (cm^{-1})	τ_2 (ps)
sym	1.2 ± 0.3	8.8 ± 1.3	3.0 ± 1.0	4.1 ± 2.0	4.1 ± 1.1	74 ± 11
antisym	1.1 ± 0.2	9.5 ± 1.4	3.8 ± 1.3	5.4 ± 2.0	6.7 ± 0.5	72 ± 9
HOD	1.0 ± 0.4	11.0 ± 1.5	4.4 ± 0.6	6.9 ± 2.1	5.3 ± 0.8	72 ± 20

[a]Note, the Δs are standard deviations. The fwhm of the inhomogeneous component of the absorption lines is the convolution (square root of the sum of the squares of the Δs) multiplied by 2.35.

dx.doi.org/10.1021/jp310086s | J. Phys. Chem. B 2013, 117, 623−635

number of systems, such as proteins,[36−38] water,[39,40] and water/salt solutions,[41] the influence of structural fluctuation of a vibrational frequency has been modeled in terms of fluctuating electric fields. Motions of the environment cause the electric field along the vibrational transition dipole direction to fluctuate, which via the Stark effect, gives rise to time-dependent frequency fluctuations.[36] In simulations, the time-dependent electric field along the vibrational transition dipole is obtained and used to calculate the electric field−electric field correlation function. The electric field−electric field correlation function is multiplied by a Stark coupling constant to give the FFCF[36,38,42,43] or an electric field/frequency map is used.[40,41]

Since the system studied here is a water molecule embedded in an environment of ions, taking the electric field picture as responsible for the spectral diffusion is useful. The results indicate that the local ion arrangement evolves on a time scale that is much faster than the overall randomization of the liquid structure, which requires randomizing the organic chains as well as the local ion configurations that give rise to the electric fields. The PF_6^- can clearly move to some extent without the butyl chains attached to the imidazolium head groups moving to any significant extent. In addition, recent experiments on alkylmethylimidazolium tetrafluoroborate show that it is possible for the imidazolium head groups to "wobble" on a much faster time scale than motions of the entire molecule including the alkyl chains.[9]

Orientational and translational motions of the anions and cations will cause the electric field along the transition dipole to vary. As mentioned above, the time scale for complete orientational relaxation of the RTIL is 2.3 ns. The FFCF shows that the variations in structure from one location to another, which give rise to the inhomogeneously broadened absorption line, randomize on a much faster time scale than the complete randomization of the RTIL. The FFCF data does not go out to sufficiently long time to rule out the possibility of a low-amplitude component (≤0.05) of the FFCF that is slower than the 70 ps τ_2 value. Therefore, all or the vast majority of configurations that influence the frequency of the hydroxyl stretches are sampled on a time scale much faster that the RTIL orientational relaxation time.

Polarization-selective pump−probe experiments were used to determine orientational relaxation times of water in the system (see eq 4). Intermode excitation transfer (discussed in detail below) contributes to both the diagonal and off-diagonal peaks that are sampled simultaneously in a pump−probe experiment. As discussed in section IV, the symmetric and antisymmetric modes of D_2O have perpendicular transition dipoles. Excitation transfer between the modes produces changes in the transition dipole directions that greatly complicate the measurement of orientational relaxation. Therefore, the measurement of orientational relaxation was made on the OD stretch of HOD (see Figure S1A in the Supporting Information). Because the OD stretch is a single mode, there are no off-diagonal excitation transfer peaks to interfere with the measurements. For the orientational relaxation measurements, 30% D_2O was used, which substantially enhances the OD peak relative to the two D_2O peaks. The orientational relaxation of HOD should be virtually identical to the orientational relaxation of D_2O in this system.

Figure 6 shows the anisotropy decay (black points) of the OD peak (2678 cm^{-1}) of HOD in $BmImPF_6$ with molar ratio of ionic liquid to total water of 24 to 1, which is the same ratio

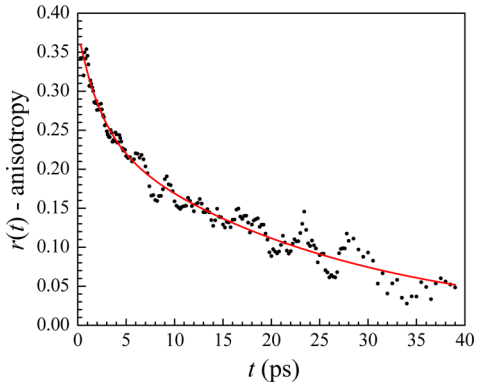

Figure 6. Anisotropy decay, $r(t)$ (black circles), of the OD stretch in a sample of 20% HOD/H_2O at a 24:1 $BmImPF_6$:water ratio. Red solid curve is a biexponential fit to the data.

used in the other experiments. The signal fits (red curve) to a biexponential decay of the form

$$r(t) = A_1 e^{-t/\tau_1^{or}} + A_2 e^{-t/\tau_2^{or}} \quad (10)$$

The fit yields $A_1 = 0.13 \pm 0.01$, $\tau_1^{or} = 2.4 \pm 0.4$ ps, $A_2 = 0.25 \pm 0.01$, and $\tau_2^{or} = 24.7 \pm 1.1$ ps. In systems such as water in very small AOT reverse micelles, in which water molecules are interacting almost exclusively with the ionic head groups, a fast component in the orientational relaxation has also been observed although the overall orientational relaxation is much slower.[44] As in previous observations on other types of systems, the fast component of orientational relaxation is assigned to wobbling in a cone.[44−47] Wobbling in a cone involves fast diffusive motions that sample a limited cone of angles. If there were no other processes, the anisotropy would decay to a plateau when all angles in the cone had been sampled. On a longer time scale, other motions relax the angular restrictions that give rise to the cone; then all angles are sampled, and the anisotropy decays to zero.[47] Using the wobbling-in-a-cone model[47] with the results from the biexponential fit yields $\tau_{wob}^{or} = 2.7 \pm 0.7$ ps and a half-cone angle $\theta_c = 29° \pm 3°$, where τ_{wob}^{or} is the time constant for the diffusive sampling of the cone of half-angle θ_c.

Fitting the orientational dynamics to such a model suggests fast limited orientational exploration of an angular potential defined by the interactions between the anions and the water molecule. The long component of orientational diffusion is 25 ps. While the anisotropy data does not decay to zero on the time scale of the experiment, the decay is close enough to zero and the slope is sufficiently steep that it is reasonable to assume that 25 ps is the time for complete orientational randomization of the HOD molecule. In bulk water, orientational relaxation occurs by jump diffusion, which is a concerted process involving many water molecules in which there is collective hydrogen bond rearrangement. Here, there is a single HOD molecule, so the bulk water mechanism cannot be operable. It is possible that the HOD undergoes a type of jump in which it switches one of the hydroxyls at a time between PF_6^- anions. It is also possible that the reorientation involves motions of the water/anions together without the water breaking a hydrogen bond with an anion. The mechanism of reorientation can be addressed through simulations.

The short-time wobbling component might also occur without the HOD breaking hydrogen bonds with the anions. NMR studies and electric field studies of water with the BF_4^-

anion, which is nominally tetrahedral, have detailed nonspecific hydrogen bonds between water and the fluorines of the BF_4^- anion.[48] Though we are unaware of any similar studies with PF_6^-, it is possible that PF_6^-, while nominally octahedral, also has nonspecific water hydrogen bonding. Then, the wobbling motion might involve the HOD "skittering" about on the surfaces of two PF_6^- anions that it is bridging via hydrogen bonds. Without breaking one or both hydrogen bonds, such skittering would have a restricted angular range.

The two orientational relaxation time constants are faster than the two FFCF spectral diffusion time constants (~5 and 70 ps). It is important to recognize that the orientational relaxation correlation function, the second Legendre polynomial correlation function, obtained from the pump−probe experiments is a different correlation function than the FFCF. Therefore, the resulting time constants cannot be directly compared. As an example, for Gaussian fluctuation orientational relaxation that is single exponential, dielectric relaxation, which measures the first Legendre polynomial correlation function, gives a time constant that is 3 times as long as that which would be measured by a pump−probe experiment on the same system.

VI. COHERENT EXCITATION EXCHANGE AND THE NATURE OF INHOMOGENEOUS BROADENING

In section IV, incoherent phonon scattering of vibrational excitation between the two D_2O stretching modes was described. At shorter time scales, excitation also oscillates back and forth between the two modes coherently after broad bandwidth IR pulses simultaneously excite both modes. This transfer is shown by the presence of beats at short times in both pump−probe and 2D IR experiments. The processes of interest are described by the diagram in Figure S2B in the Supporting Information called "Inter-Mode One Quantum Transitions," labeled *j*. Diagrams of this type where both vibrational modes are excited during the waiting time, T_w, give rise to beats and can occur in both the diagonal and off-diagonal peaks. The oscillations are due to the differences in the oscillating phase factors of the two states[49−51] and occur at a frequency of $\omega_{as} = \omega_a - \omega_s = 99\ cm^{-1}$. We focus on the diagrams (quantum pathways) that give rise to the off-diagonal peaks, $s \rightarrow a$ and $a \rightarrow s$ in Figure 2A. These off-diagonal peaks have contributions from three diagrams (quantum pathways), two of which are rephasing and one is nonrephasing. However, only one of the diagrams, a rephasing diagram, produces beats. Though diagrams involving the incoherent exchange of energy contribute to this peak, their contribution is negligible on the time scale of the observed oscillations (see section IV).

Figure 7 shows the short time pump−probe data (black curves) for the symmetric stretching mode ($2627\ cm^{-1}$) and a fit to the data (red curves). Because of the large nonresonant signal, the data begin at 200 fs. The oscillations ride on top of the population relaxation discussed in section IV. The overall population relaxation (see Figure 3) was subtracted out to more clearly show the oscillatory behavior. Figure 7A is the data with the probe polarization perpendicular to the pump and 7B is the data with the probe polarization parallel. Because this is a pump−probe experiment, both the off-diagonal ($a \rightarrow s$) and the diagonal ($1s$) bands contribute to the signal (see Figure 2A). Both peaks have signal contributions to the observed oscillations; the oscillatory component in the diagonal peak comes from a nonrephasing pathway. The equivalent data are observed at the wavelength corresponding to the antisymmetric mode.

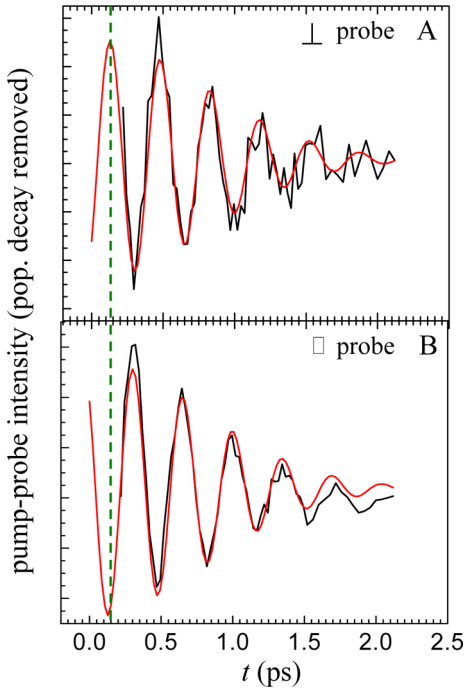

Figure 7. Symmetric mode perpendicular probe (A) and parallel probe (B) pump−probe data (black curves). The red curves are fits to the data. The dashed green line is a guide to the eye to show that the populations reach maxima 180° out of phase from one another. The oscillations are the result of coherent excitation exchange between two modes with perpendicularly oriented transition dipoles.

As is evident from Figure 7, the beats damp rapidly. Experiments in the visible have mainly attributed this damping to homogeneous dephasing, although recently inhomogeneous broadening of electronic transitions has also been considered.[52−54] Homogeneous dephasing is determined by a Lorentzian homogeneous component of the absorption line, which gives rise to an exponential decay (see just below eq 6). From the 2D IR vibrational echo experiments, we know the homogeneous line widths (see Table 2). When the damping was modeled using the homogeneous exponential decay, it was found to be much slower than observed experimentally.

Damping can also be caused by inhomogeneous broadening of the absorption lines as described below. Therefore, the damping of the oscillations occurs from both the homogeneous and inhomogeneous contributions to the transitions. From the FFCF parameters (Table 2), the homogeneous and inhomogeneous contributions to the antisymmetric and symmetric spectral lines are known. As both lines have significant homogeneous (Lorentzian) and inhomogeneous (Gaussian) components, the envelope of the damped sinusoid is expected to be the Fourier transform of a Voigt (the convolution of a Lorentzian and Gaussian line shape). In the time domain, the Voigt profile gives rise to an envelope decay that is the product of Gaussian and exponential decays. The pump−probe data (Figure 7) were fit to a sinusoidal wave damped by the Gaussian-exponential product decay

$$I(t) = y_0 + Ae^{-t^2/(2\sigma_{damp}^2)}e^{-t/T_2}\cos(2\pi\nu t + \phi) \qquad (11)$$

σ_{damp} is the temporal standard deviation of the Gaussian damping function (ps), T_2 is the homogeneous dephasing time

dx.doi.org/10.1021/jp310086s | J. Phys. Chem. B 2013, 117, 623−635

Table 3. Pump−Probe Fit Parameters for the Symmetric and Antisymmetric Stretching Modes of D_2O in $BmImPF_6$[a]

	ν (ps^{-1})	σ_{damp} (ps)	σ_{damp} (cm^{-1})[b]	fwhm (cm^{-1})
symmetric				
parallel	2.9 ± 0.2	1.15 ± 0.11	4.6 ± 0.6	10.9 ± 1.4
perpendicular	2.8 ± 0.2	1.68 ± 0.15	3.2 ± 0.8	7.4 ± 1.9
antisymmetric				
parallel	3.0 ± 0.2	1.16 ± 0.26	4.9 ± 1.4	11.6 ± 3.2
perpendicular	2.8 ± 0.2	1.12 ± 0.15	4.6 ± 0.8	10.8 ± 1.8

[a]The σ_{damp} (cm^{-1}) is the Fourier transform of the damping time constant in ps. Fwhm (cm^{-1}) is 2.355 times σ_{damp} (cm^{-1}) and listed to give a reference for the line widths of the coherently transferring mode. [b]σ_{damp} (cm^{-1}) is the Fourier transform of σ_{damp} (ps) after it is converted from radians/s to cm^{-1}.

(ps) fixed to the experimentally determined value, ν is the beat frequency (ps^{-1}), and ϕ is a phase factor. ϕ is used to account for $t = 0$ not being perfectly defined because of the finite pulse durations.

The pump−probe oscillations probed with the two polarizations are 180° out of phase (see Figure 7) because the transition dipoles of the two modes are perpendicular. In the absence of oscillations, probing perpendicular on a time scale very short compared to orientational relaxation will produce a smaller signal than probing parallel. When population transfers from the antisymmetric mode to the symmetric mode (data in Figure 7) replacing the population that transfers out, it will come in with perpendicular polarization, so perpendicular probing will show an initial increase in signal. This increase then oscillates up and down. When probing parallel, the opposite happens and the oscillation is down and up.

The damping of the oscillations as described by eq 11 gives the standard deviation of the time domain Gaussian damping. Table 3 lists the oscillation frequencies and the damping constants from the pump−probe data for both the symmetric and antisymmetric modes probed parallel and perpendicular. Within experimental error, the oscillation frequencies are the same, as would be expected, and are equal to the splitting between the two absorption peaks shown in Figure 1. Fourier transformation of the time domain Gaussian gives the frequency domain Gaussian, which is the inhomogeneous width that contributes to the damping. In Table 3, the standard deviation is given for the frequency domain Gaussian as σ_{damp} in cm^{-1} and as the fwhm also in cm^{-1}. The width of the inhomogeneous distribution that contributes to the damping of the oscillations is ∼8−10 cm^{-1}, which is slightly less than or equal to the total inhomogeneous line widths (see Table 2). The nature of the inhomogeneous broadening and the relationship between inhomogeneous frequencies in the two modes is discussed below.

Figure 8A shows 2D IR spectra of the $s \rightarrow a$ coherence transfer peak (see Figure 2) at short T_ws. The red line shown on each spectrum is the center line discussed in section V. The change in slope of the center line (CLS) is directly related to frequency correlations (the FFCF) over a time period T_w.[7,8] At long times, the shape of this peak as well as other peaks will change because of spectral diffusion. As spectral diffusion proceeds, the CLS will approach zero. At very short times, it is evident from Figure 8A that the CLS is oscillatory. Figure 8B is a plot of the CLS vs T_w for times very short compared to the time scales for spectral diffusion. The data shows that the CLS oscillates and the oscillations decay rapidly. Similar data were collected for the symmetric and antisymmetric diagonal peaks (Figure S4 in the Supporting Information). The results of the oscillating CLS fits using eq 11 are given in Table 4. Within

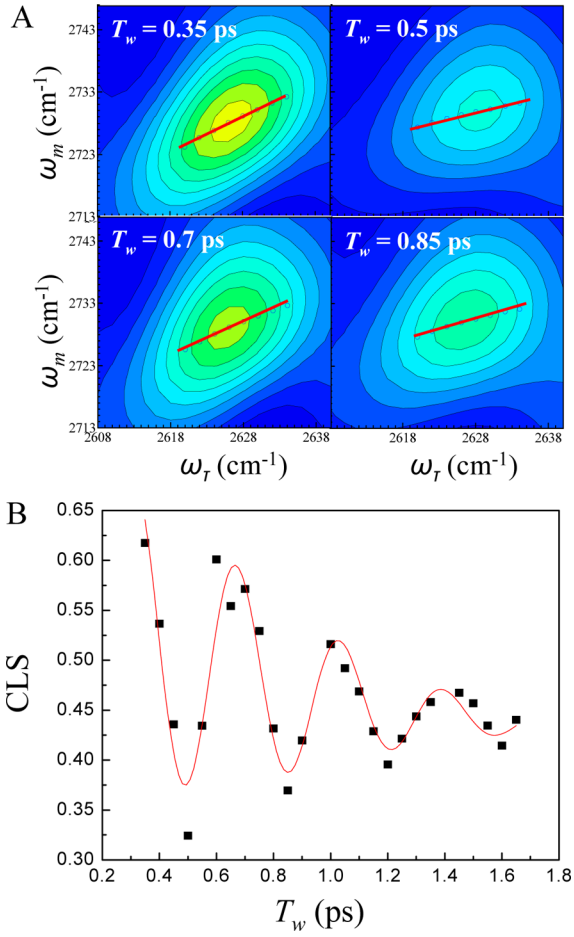

Figure 8. Shape oscillations of the 2D IR spectra from coherent excitation transfer between the two modes. (A) Progression of the shape of the $s \rightarrow a$ 2D cross peak as a function of T_w. The cross peak exhibits oscillations in the CLS (red lines). (B) CLS is plotted as a function of T_w for the $s \rightarrow a$ cross peak (black squares). The red curve is a fit to the data.

Table 4. CLS Fit Parameters for the Symmetric and Antisymmetric Stretching Modes of D_2O and the OD Stretch of Dilute HOD in $BmImPF_6$

	ν (ps^{-1})	σ_{damp} (ps)
$s \rightarrow a$ cross peak	2.7 ± 0.2	1.12 ± 0.35
sym diagonal	2.6 ± 0.2	1.34 ± 0.42
antisym diagonal	2.8 ± 0.2	0.98 ± 0.34

experimental error, the frequencies and the Gaussian damping constants are the same as those obtained from the pump−

dx.doi.org/10.1021/jp310086s | J. Phys. Chem. B 2013, 117, 623−635

probe experiments. However, the CLS oscillations reflect shape changes rather than amplitude changes. The agreement between the two types of experiments is consistent with simulations of 2D electronic spectra of coupled chromophores.[51]

Qualitatively, peak shape oscillations as reflected by the change in the CLS can be understood in terms of the nature of the correlation of the inhomogeneous broadening in the symmetric and antisymmetric modes. One extreme is that the inhomogeneous broadening of the two lines is completely correlated. Complete correlation means that a frequency on the red side of one line will transfer to the equivalent frequency on the red side of the other mode's line. For example, if a particular molecule has its symmetric stretch frequency one standard deviation to the red of line center, when it transfers to the antisymmetric mode, the frequency is also one standard deviation to the red. If this was true for all frequencies across the inhomogeneously broadened lines, then there would be no shape change upon coherent excitation transfer.

Another possibility is that there is no correlation in the frequencies of the two modes. A single transition frequency in the inhomogeneous line of a mode does not imply that all molecules with this frequency have identical environments and interactions with their surroundings. Various local differences in the surroundings can play off against each other and give rise to a coincidental degeneracy of vibrational frequncies.[55] Consider a subensemble of molecules that all have the same transition frequency in the initial mode. When the excitation is transferred to the other mode, each molecule's interaction with their new mode's local environments is different, and the subensemble no longer has identical transition frequencies. Complete lack of correlation means that the molecules in a subensemble of a single frequency in one mode will distribute among all frequencies across the line upon excitation transfer to the other mode. If there is no correlation, the beating component of the CLS (one of three contributions (diagrams) to the off-diagonal peak) would oscillate between its initial value at very short time with a slope determined by the extent of homogeneous broadening and a slope of zero after half a cycle. That is, the oscillating component of the peak shape will oscillate between a peak elongated along the diagonal at short time and a round peak shape after a half-cycle. This oscillating component is combined with the two nonoscillating contributions to give an observed change that is less than that of the oscillating component by itself.

The third limiting case is complete anticorrelation. Anticorrelation means that a frequency on the red side of the line of one mode undergoes excitation exchange to the equivalent frequency on the blue side of the line of the other mode. For example, a subensemble with a frequency that is initially one standard deviation to the red of the peak of the symmetric mode will undergo excitation transfer to a frequency that is one standard deviation to the blue in the antisymmetric mode. In this case, the oscillating component of the CLS will go from its initial value at short time to the negative of this value one-half-cycle later. At short time, the oscillating component is elongated along the diagonal, and a half-cycle later, it will be elongated to the same extent along a line that is perpendicular to the diagonal.

The data shown in Figure 8 for the $s \rightarrow a$ coherence transfer peak has contributions from three quantum pathways, a nonrephasing and rephasing diagram which do not oscillate and one rephasing diagram that oscillates. Although the CLS has been shown to additively reflect the sum of its component contributions,[56] we cannot directly extract the degree of frequency correlation in the oscillating rephasing component by examining its CLS. Without a nonrephasing diagram to "balance out" the rephasing diagram,[57] the oscillating peak shape has a phase twist which obscures the degree of frequency correlation in the oscillating peak shape's CLS.

To obtain a qualitative understanding of the nature of the inhomogeneous broadening that is responsible for the shape oscillation, we employ numerical modeling of the cross-peak line shape. The line shape was calculated using the FFCF parameters (section V) of the antisymmetric and symmetric line shapes to numerically model different possible limits of frequency correlation in the off-diagonal line shape (see Supporting Information). These scenarios map the degree of correlation in the oscillating rephasing component (highly correlated, uncorrelated, and anticorrelated) to the calculated peak's CLS values. In the calculations, the FFCF parameters for both the symmetric and antisymmetric lines were used, which provide the range of possible values.

The model calculations yield line shapes at T_w = 0.35 ps (prior to oscillation) with CLS values between 0.51 and 0.66. The experimental value at this time is 0.62 (Figure 8B). At T_w = 0.5 ps where the CLS is at its minimum, the CLS has a value from the fit to the experimental data of 0.37. This CLS value was compared to calculated spectra which are the combination of two nonoscillating and one oscillating component. For the fully correlated model, there is no oscillation. Using the uncorrelated model for the oscillating component gives a CLS between 0.42 and 0.55 for the total calculated spectrum. The anticorrelated model for the oscillating component gives a CLS of ∼0 for the total spectrum (see the Supporting Information). The experimental off-diagonal peak CLS minimum value is ∼0.37, which is between the values calculated with the uncorrelated and anticorrelated scenarios. These results suggest that the CLS value at the minimum reflects some degree of frequency anticorrelation between the symmetric and antisymmetric modes. The fully uncorrelated model cannot produce a small enough value of the CLS by itself to match the experimental results, and the experimental CLS value is too big to be consistent with the fully anticorrelated model.

To determine an underlying reason for the observed partial anticorrelation between the two modes, we first numerically examined the effect of anticorrelation of the local hydroxyl modes in creating anticorrelated, antisymmetric, and symmetric modes.[58] Numerical calculations were performed using a variety of anticorrelated local mode frequencies within a range determined by the inhomogeneous width of the OD local mode of HOD (see Figure S1 in the Supporting Information and Table 2) and a fixed value of the coupling constant, J = −50 cm^{-1} (see eq 7a). It was found that anticorrelation of the local modes could produce only an insignificant contribution to inhomogeneous broadening, at most ∼1 cm^{-1}. In addition, there is no physical reason why the two local OD modes on D_2O molecules would have their frequencies anticorrelated.

The mechanism that can result in nonnegligible anticorrelation of mode frequencies is environment-induced variations in the coupling constant J (see eq 7b). Larger J results in a bigger splitting, and smaller J produces a reduced splitting. If the distribution of J values was the sole source of inhomogeneous broadening, the result would be perfect anticorrelation of the two modes, which is not the case.

dx.doi.org/10.1021/jp310086s | J. Phys. Chem. B 2013, 117, 623−635

The partial anticorrelation deduced from the oscillating CLS data (Figure 8) can be explained by a combination of inhomogeneous broadening mechanisms. One contribution is a distribution in coupling constants, J, which results in some degree of anticorrelation. The other contribution is the direct influence of a variety of environments creating a distribution of symmetric and antisymmetric mode frequencies. The fact that the inhomogeneous widths of the two stretching modes are different shows that the direct interactions of the two modes with their environment differ. Different interactions suggest that the direct influence component of the inhomogeneous broadening is not completely correlated. Thus, inhomogeneous broadening in this system can be viewed as follows. There is a contribution to the inhomogeneous broadening that arises from variation in the local mode coupling J. It was determined in ref 10 that fluctuations in J for water in acetonitrile were ~4 cm^{-1}. The structural fluctuations are much slower in this $BmImPF_6$ system, so variations in J are basically static on the time scale of the oscillations and are a manifestation of the inhomogeneity of local environments. Each J produces a splitting between the modes. In addition, there is a distribution of frequencies that is determined by direct environmental effects on the eigenmode frequencies. On a longer time scale than the oscillations shown in Figure 8, spectral diffusion will randomize both the J and direct distributions.

VII. CONCLUDING REMARKS

Two-dimensional infrared spectroscopy and polarization sensitive pump−probe experiments were used to investigate the inter- and intramolecular dynamics of D_2O and HOD in the room temperature ionic liquid, $BmImPF_6$. The heavy water and HOD were in such low concentration that the individual water molecules are isolated from each other. Therefore, the water molecules interact with ions but not with other water molecules.

In the absorption spectrum of D_2O in $BmImPF_6$, the symmetric and antisymmetric hydroxyl stretching vibrational modes produce narrow, well-resolved lines (see Figures 1 and Figure S1 in the Supporting Information). The splitting of the D_2O lines gives the coupling between the local modes that give rise to the two eigenstates. The 2D IR spectrum has diagonal and off-diagonal bands that provide additional spectroscopic information (see Figure 2). Peak positions in the 2D IR spectrum provide the combination band shift, the anharmonicities of the two eigenstates, as well as the anharmonicity of the OD stretch of HOD.

Spectral diffusion measurements (see Figure 5) give information on the structural evolution of the water−RTIL system. Both modes of D_2O and the OD stretch of HOD yield essentially the same spectral diffusion dynamics. In addition to a homogeneous component, two time scales are observed for the spectral diffusion, ~5 and ~70 ps. The slow component is the time for complete structural randomization of those degrees of freedom of the liquid that contribute to the inhomogeneous width of the absorption bands. The 70 ps time is much faster than the time for complete orientational randomization of the ionic liquid, 2.3 ns. For comparison, the orientational relaxation time of the water molecules in the RTIL system is 25 ps (see Figure 6).

In the 2D IR spectrum of D_2O, several bands grow in with increasing time (see Figure 4). The growth is caused by incoherent scattering of excitations between the symmetric and antisymmetric stretching modes. The growth of the bands yields the up and down scattering time constant of 7.8 and 4.4 ps, respectively. These time constants obey detailed balance.

Coherent excitation exchange between the two modes occurs on a much faster time scale. Pump−probe experiments performed on the symmetric and antisymmetric peaks show very rapid (~300 fs) oscillations in amplitude (see Figure 7). The damping of the oscillations occurs because of a combination of homogeneous and inhomogeneous broadening. The data is well described by the product of a Fourier transform of a Voigt line shape function and a sine wave. The inhomogeneous widths obtained from fitting the damping are close to but somewhat less than the entire inhomogeneous line widths.

The 2D IR spectra also shows short time shape oscillations, which are quantified in terms of the CLS (see Figure 8). The shape oscillates between elongated along the diagonal at very short time to less elongated, and then back to more elongated. The oscillation in shape reflects oscillation in the frequency correlation between the frequencies initially excited by pulse 1 and the frequencies associated with the vibrational echo emission. The experimental CLS values were compared to those obtained from calculated spectra with varying degrees of inhomogeneous frequency correlation between the symmetric and antisymmetric lines. The results are consistent with frequencies that have a significant degree of anticorrelation as well a substantial component in which the frequencies of the two lines are uncorrelated. The anticorrelation is attributed to variations in the coupling between the two local modes that give rise to the symmetric and antisymmetric eigenstates.

■ ASSOCIATED CONTENT

Supporting Information

FT-IR comparison between the HOD of water in $BmImPF_6$ with that of bulk water, an explanation of the interaction pathways using double-sided rephasing Feynman diagrams, and information on the calculation of the cross peak to model the CLS for limiting cases of frequency correlation. This material is available free of charge via the Internet at http://pubs.acs.org.

■ AUTHOR INFORMATION

Corresponding Author

*E-mail: fayer@stanford.edu.

Present Address

[†]Current Address: Lincoln Laboratory, Massachusetts Institute of Technology, Lexington, MA 02420.

Notes

The authors declare no competing financial interest.

■ ACKNOWLEDGMENTS

We thank the Department of Energy (DE-FG03-84ER13251) for support of this research. We also thank the National Science Foundation (CHE-1157772), which supported the optical heterodyne detected optical Kerr effect measurements. D.B.W. thanks Stanford for a Graduate Research Fellowship. We also thank Praveen Chowdary, Aaron Kelly, and Amr Tamimi for helpful discussions.

■ REFERENCES

(1) Park, S.; Fayer, M. D. *Proc. Natl. Acad. Sci. U.S.A.* **2007**, *104*, 16731−16738.

(2) Tielrooij, K. J.; van der Post, S. T.; Hunger, J.; Bonn, M.; Bakker, H. J. *J. Phys. Chem. B* **2011**, *115*, 12638−12647.

(3) Giammanco, C. H.; Wong, D. B.; Fayer, M. D. *J. Phys. Chem. B* **2012**, *116*, 13781−13792.
(4) Danten, Y.; Cabaco, M. I.; Besnard, M. *J. Phys. Chem. A* **2009**, *113*, 2873−2889.
(5) Cammarata, L.; Kazarian, S. G.; Salter, P. A.; Welton, T. *Phys. Chem. Chem. Phys.* **2001**, *3*, 5192−5200.
(6) Masaki, T.; Nishikawa, K.; Shirota, H. *J. Phys. Chem. B* **2010**, *114*, 6323−6331.
(7) Kwak, K.; Park, S.; Finkelstein, I. J.; Fayer, M. D. *J. Chem. Phys.* **2007**, *127*, 124503.
(8) Kwak, K.; Rosenfeld, D. E.; Fayer, M. D. *J. Chem. Phys.* **2008**, *128*, 204505.
(9) Sturlaugson, A. L.; Fruchey, K. S.; Fayer, M. D. *J. Phys. Chem. B* **2012**, *116*, 1777−1787.
(10) Jansen, T. L. C.; Cringus, D.; Pshenichnikov, M. S. *J. Phys. Chem. A* **2009**, *113*, 6260.
(11) Cringus, D.; Jansen, T. L. C.; Pshenichnikov, M. S.; Wiersma, D. A. *J. Chem. Phys.* **2007**, *127*, 084507.
(12) Fenn, E. E.; Wong, D. B.; Fayer, M. D. *J. Chem. Phys.* **2011**, *134*, 054512.
(13) Koddermann, T.; Wertz, C.; Heintz, A.; Ludwig, R. *Angew. Chem., Int. Ed.* **2006**, *45*, 3697.
(14) Smith, J. D.; Saykally, R. J.; Geissler, P. L. *J. Am. Chem. Soc.* **2007**, *129*, 13847−13856.
(15) Danten, Y.; Cabaco, M. I.; Besnard, M. *J. Phys. Chem. A* **2009**, *113*, 2873−2889.
(16) Danten, Y.; Cabaco, M. I.; Besnard, M. *J. Mol. Liq.* **2010**, *153*, 57−66.
(17) Feng, S.; Voth, G. A. *Fluid Phase Equilib.* **2010**, *294*, 148−156.
(18) Hamm, P.; Lim, M.; Hochstrasser, R. M. *J. Phys. Chem. B* **1998**, *102*, 6123.
(19) Mukamel, S. *Annu. Rev. Phys. Chem.* **2000**, *51*, 691−729.
(20) Wright, J. C. *Int. Rev. Phys. Chem.* **2002**, *21*, 185−255.
(21) Fayer, M. D. *Annu. Rev. Phys. Chem.* **2008**, *60*, 21−38.
(22) Khalil, M.; Tokmakoff, A. *Chem. Phys.* **2001**, *266*, 213−230.
(23) Cohen-Tannoudji, C.; Diu, B.; Laloe, F. *Quantum Mechanics*; Wiley-Interscience: Paris, 2006; Vol. *1*.
(24) Cho, M.; Fleming, G. R. *J. Chem. Phys.* **2005**, *123*, 114506.
(25) Hamm, P.; Zanni, M. *Concepts and Methods of 2d Infrared Spectroscopy*; Cambridge University Press: Cambridge, UK, 2011.
(26) Golonzka, O.; Khalil, M.; Demirdoven, N.; Tokmakoff, A. *J. Chem. Phys.* **2001**, *115*, 10814−10828.
(27) Khalil, M.; Demirdoven, N.; Tokmakoff, A. *J. Phys. Chem. A.* **2003**, *107*, 5258−5279.
(28) Mukamel, S. *Principles of Nonlinear Optical Spectroscopy*; Oxford University Press: New York, 1995.
(29) Kenkre, V. M.; Tokmakoff, A.; Fayer, M. D. *J. Chem. Phys.* **1994**, *101*, 10618.
(30) Moilanen, D. E.; Fenn, E. E.; Wong, D.; Fayer, M. D. *J. Phys. Chem. B* **2009**, *113*, 8560−8568.
(31) Sarangi, S. S.; Reddy, S. K.; Balasubramanian, S. *J. Phys. Chem. B* **2011**, *115*, 1874−1880.
(32) Fumino, K.; Wulf, A.; Ludwig, R. *Angew. Chem.* **2008**, *47*, 3830−3834.
(33) Asbury, J. B.; Steinel, T.; Kwak, K.; Corcelli, S. A.; Lawrence, C. P.; Skinner, J. L.; Fayer, M. D. *J. Chem. Phys.* **2004**, *121*, 12431−12446.
(34) Asbury, J. B.; Steinel, T.; Stromberg, C.; Corcelli, S. A.; Lawrence, C. P.; Skinner, J. L.; Fayer, M. D. *J. Phys.Chem. A* **2004**, *108*, 1107−1119.
(35) Nicolau, B. G.; Sturlaugson, A.; Fruchey, K.; Ribeiro, M. C. C.; Fayer, M. D. *J. Phys. Chem. B* **2010**, *114*, 8350−8356.
(36) Williams, R. B.; Loring, R. F.; Fayer, M. D. *J. Phys. Chem. B* **2001**, *105*, 4068−4071.
(37) Merchant, K. A.; Noid, W. G.; Akiyama, R.; Finkelstein, I.; Goun, A.; McClain, B. L.; Loring, R. F.; Fayer, M. D. *J. Am. Chem. Soc.* **2003**, *125*, 13804−13818.
(38) Bagchi, S.; Nebgen, B. T.; Loring, R. F.; Fayer, M. D. *J. Am. Chem. Soc.* **2010**, *132*, 18367−18376.
(39) Eaves, J. D.; Tokmakoff, A.; Geissler, P. L. *J. Phys. Chem. A* **2005**, *109*, 9424−9436.
(40) Corcelli, S. A.; Lawrence, C. P.; Asbury, J. B.; Steinel, T.; Fayer, M. D.; Skinner, J. L. *J. Chem. Phys.* **2004**, *121*, 8897−8900.
(41) Lin, Y.-S.; Auer, B. M.; Skinner, J. L. *J. Chem. Phys.* **2009**, *131*, 144511.
(42) Finkelstein, I. J.; Goj, A.; McClain, B. L.; Massari, A. M.; Merchant, K. A.; Loring, R. F.; Fayer, M. D. *J. Phys. Chem. B* **2005**, *109*, 16959−16966.
(43) Merchant, K. A.; Thompson, D. E.; Xu, Q. H.; Williams, R. B.; Loring, R. F.; Fayer, M. D. *Biophys. J.* **2002**, *82*, 3277−3288.
(44) Moilanen, D. E.; Fenn, E. E.; Wong, D.; Fayer, M. D. *J. Chem. Phys.* **2009**, *131*, 014704.
(45) Wang, C. C.; Pecora, R. *J. Chem. Phys.* **1980**, *72*, 5333−5340.
(46) Lipari, G.; Szabo, A. *Biophys. J.* **1980**, *30*, 489−506.
(47) Tan, H.-S.; Piletic, I. R.; Fayer, M. D. *J. Chem. Phys.* **2005**, *122*, 174501.
(48) Akitt, J. W. *J. Chem. Soc., Faraday Trans. 1* **1975**, *71*, 1557−1572.
(49) Merchant, K. A.; Thompson, D. E.; Fayer, M. D. *Phys. Rev. A* **2002**, *65*, 023817(023816).
(50) Khalil, M.; Demirdoven, N.; Tokmakoff, A. *J. Chem. Phys.* **2004**, *121*, 362−373.
(51) Cheng, Y. C.; Engel, G. S.; Fleming, G. R. *Chem. Phys.* **2007**, *341*, 285−295.
(52) Ishizaki, A.; Fleming, G. R. *J. Phys. Chem. B* **2011**, *115*, 6227−6233.
(53) Caram, J. R.; Lewis, N. H. C.; Fidler, A. F.; Engel, G. S. *J. Chem. Phys.* **2012**, *136*, 104505.
(54) Pelzer, K. M.; Griffin, G. B.; Gray, S. K.; Engel, G. S. *J. Chem. Phys.* **2012**, *136*, 164508.
(55) Lee, H. W. H.; Walsh, C. A.; Fayer, M. D. *J. Chem. Phys.* **1985**, *82*, 3948−3958.
(56) Fenn, E. E.; Fayer, M. D. *J. Chem. Phys.* **2011**, *135*, 07450.
(57) Khalil, M.; Demirdoven, N.; Tokmakoff, A. *Phys. Rev. Lett.* **2003**, *90*, 047401(047404).
(58) Thompson, D. E.; Merchant, K. A.; Fayer, M. D. *Chem. Phys. Lett.* **2001**, *340*, 267−274.